ADVANCED FUNCTIONAL MATERIALS

Supporting Information

for *Adv. Funct. Mater.,* DOI: 10.1002/adfm.202105384

Conjugated Porous Polymers Based on BODIPY and BOPHY Dyes in Hybrid Heterojunctions for Artificial Photosynthesis

Laura Collado, Teresa Naranjo, Miguel Gomez-Mendoza, Carmen G. López-Calixto, Freddy E. Oropeza, Marta Liras,* Javier Marugán,* and Víctor A.de la Peña O'Shea**

SUPPORTING INFORMATION

Conjugated porous polymers based on BODIPY and BOPHY dyes in hybrid heterojunctions for artificial photosynthesis

Laura Collado[a,b,*], Teresa Naranjo[a], Miguel Gomez-Mendoza[a], Carmen G. López-Calixto[a], Freddy Oropeza[a], Marta Liras[a,*], Javier A. Marugán[b,*], Víctor A. de la Peña O'Shea[a*]

[a]Photoactivated Processes Unit, IMDEA Energy Institute, Parque Tecnológico de Móstoles, Avda. Ramón de la Sagra 3, 28935 Móstoles, Madrid, Spain.
[b]Department of Chemical and Environmental Technology, ESCET, Universidad Rey Juan Carlos, C/ Tulipán s/n, 28933 Móstoles, Madrid, Spain.

Corresponding authors:

laura.collado@urjc.es (Laura Collado)
marta.liras@imdea.org (Marta Liras)
javier.marugan@urjc.es (Javier A. Marugán)
victor.delapenya@imdea.org (Víctor A. de la Peña O'Shea)

SUPPORTING INFORMATION CONTENTS

Page

Figure S1. Emission spectra of the irradiation sources used in the photocatalytic tests: (**A**) Hg-lamp for water splitting; (**B**) UV lamps (four 6W lamps, λ_{max}=369 nm, average intensity of 47.23Wm^{-2}) and (**C**) visible light source (30W white LED, average intensity 53.89Wm^{-2} in the region 400–600 nm) for CO_2 photoreduction tests. 4

Figure S2. Thermogravimetric analyses of **CMPBDP@T-10** (**A**) and **IEP-7@T-10** (**B**) hybrids under 80 ml min^{-1} air flow. 5

Figure S3. N_2 adsorption/desorption isotherms and BET surface areas of CPPs (**A**-**B**) and CPP@TiO_2 hybrids (**C**-**D**). 6

Figure S4. ATR-FTIR spectra of the polymeric networks **IEP-7** and **CMPBDP**. 7

Figure S5. Solid ^{13}C-NMR spectra of **CMPBDP@T-10** (**A**) and **IEP-7@T-10** (**B**) hybrids. 8

Figure S6. XPS of hybrid samples in the F 1s and N 1s regions before and after a photocatalytic H_2 evolution experiment. 9

Figure S7. STEM images of **Pt/CMPBDP@T-10** hybrid. **B** and **C** depicts a magnification of the squared regions in image A; **D** shows the HAADF-STEM image from C; **F** shows the EDS spectrum from region E. 10

Figure S8. A) Cyclic voltammetry (CV) of **CMPBDP** measured in acetonitrile containing 0.1M [(^{n}Bu)$_4$)N]PF_6 as electrolyte at a scan rate of 20 mV s^{-1}; **B**) Experimental band energy diagram obtained for CPPs and TiO_2 (note that CV for **IEP-7** and TiO_2 can be found in previous publications[1]), including the water-splitting and CO_2/CH_4 redox couples at pH = 0. 11

Figure S9. H_2 and CO evolution over the **CMPBDP@T-10** hybrid under different reaction atmospheres (i.e. Ar; Ar + H_2O; CO_2 + H_2O) after15 h of UV illumination. 12

Figure S10. Cumulative hydrogen production *versus* reaction time of CPPs and TiO_2 under UV illumination. 13

Figure S11. Recyclability of **CMPBDP@T-10** for H_2 production during UV-dark cycles. 14

Figure S12. ATR-FTIR spectra of **CMPBDP@T-10** before and after 3 UV-dark cycles of photocatalytic H_2 evolution tests. 15

Figure S13. Normalized fluorescence decay traces (λ_{exc} = 372 nm, cut-off filter centered at 450 nm) for TiO_2 (**A**) and the hybrids **CMPBDP@T-10** (**B**) and **IEP-7@T-10** (**C**) measured in solid state. The fitting curves (red) have been included in all cases. 16

Figure S14. (**A**) Transient absorption spectra (TAS, λ_{exc} = 355 nm) for TiO_2 measured in suspension solution under inert atmosphere. (**B**) TAS for TiO_2 (grey), the hybrids **CMPBDP@T-10** (green) and **IEP-7@T-10** (blue), and the comparison with their bare materials **CMPBDP** and **IEP-7** (magenta and cyan, respectively) under the same conditions. 17

Figure S15. Fits of the normalized transient decay traces (λ_{exc} = 355 nm, λ_{mon} = 460 nm) monitored up to 400 ns after laser pulse (left side) or until 6 μs (right side) for **A**) TiO_2, **B**) **CMPBDP@T-10** and **C**) **IEP-7@T-10**. 18

Figure S16. Decay traces (λ_{exc} = 355 nm, λ_{obs} = 460 nm) for deaerated TiO_2 in the absence (red) or presence (black) of 10% vol. MeOH aqueous suspensions. 19

Figure S17. A) TAS (λ_{exc} = 355 nm) for TiO_2 in the absence (grey, open circles) or in the presence (black circles) of H_2PtCl_6 as electron scavenger. TAS for **CMPBDP@T-10** (green) and **IEP-7@T-10** (blue) in the presence of H_2PtCl_6 have been included for comparative purposes; **B**) Decay traces (λ_{exc} = 355 nm, λ_{obs} = 460 nm) for deaerated TiO_2 in absence (grey) or presence (black) of H_2PtCl_6. 20

Figure S18. Solid-state photoluminescence spectra of **CMPBDP** (λ_{exc} = 445 nm, cut-off filter at 450 nm). 21

Table S1. Surface composition of **CMPBDP@T-10** based on X-ray photoelectron spectra before and after a photocatalytic H_2 production test. 22

Table S2. Cumulative CO_2 photoreduction productions after 15 h of UV illumination for hybrid heterojunctions (i.e. **CMPBDP@T-10**, **IEP-7@T-10**), bare polymer (i.e. **CMPBDP**) and TiO_2. Photonic efficiencies towards CH_4 are also included for comparison. 23

Table S3. Some relevant examples of organic-inorganic hybrid materials based on TiO_2 and polymers for CO_2 photoreduction. 24

Table S4. Some relevant examples of organic-inorganic hybrid materials based on TiO_2 for the photocatalytic hydrogen production from water. 26

REFERENCES 28

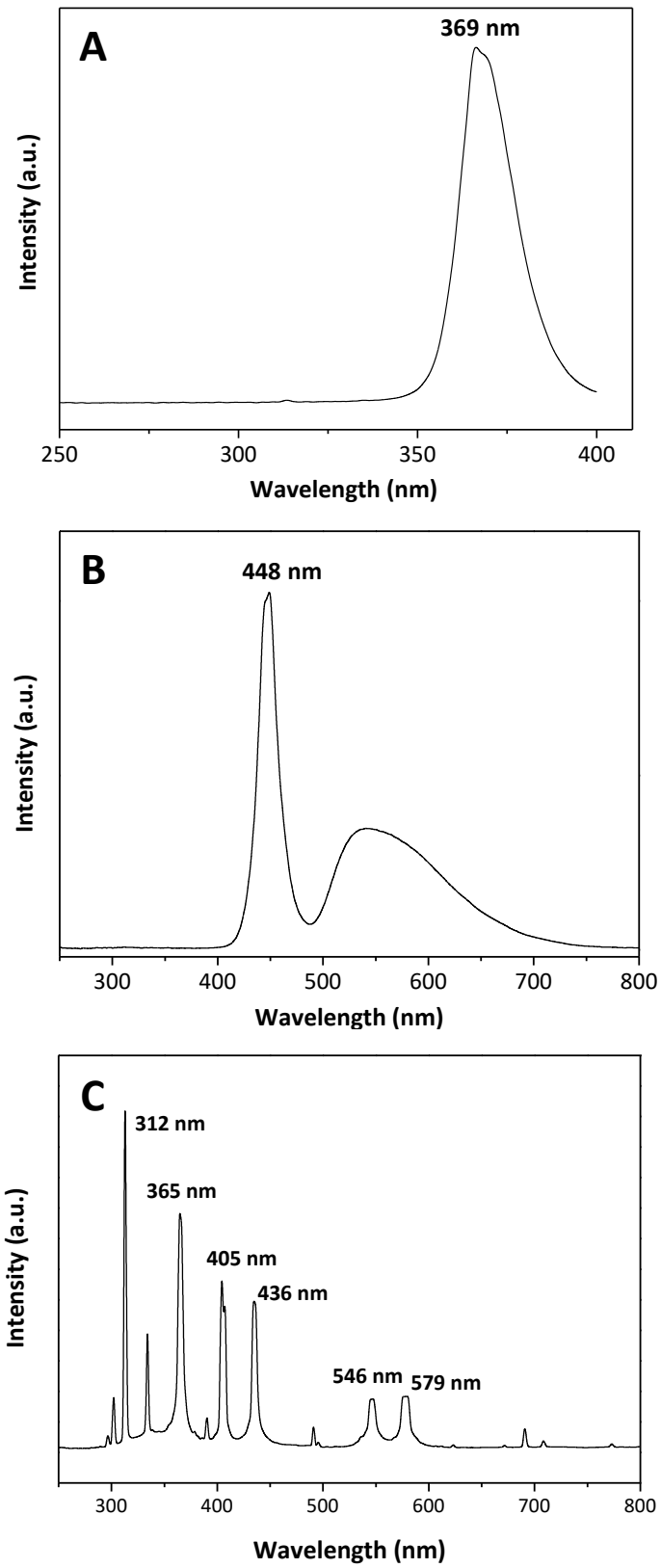

Figure S1. Emission spectra of the irradiation sources used in the photocatalytic tests: **A**) UV lamps (four 6W lamps, λ_{max}=369 nm, average intensity of 47.23Wm^{-2}); **B**) Visible light source (30W white LED, average intensity 53.89Wm^{-2} in the region 400–600 nm) for CO_2 photoreduction tests and **C**) 150 W medium-pressure Hg immersion lamp for water splitting.

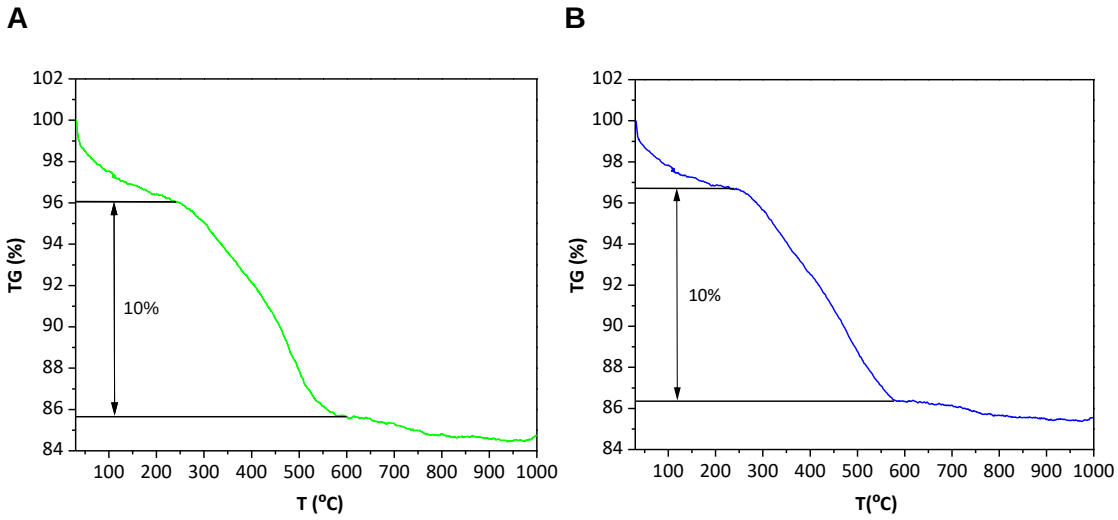

Figure S2. Thermogravimetric analyses of **CMPBDP@T-10** (**A**) and **IEP-7@T-10** (**B**) hybrids under 80 ml min^{-1} air flow.

The thermogravimetric analyses of both hybrids under air atmosphere show a weight loss of *ca*. 10 wt.% in the range 230 °C-600 °C, which correspond to the decomposition of the polymers. The initial weight loss at temperatures lower than 230 °C is associated to the removal of solvents.

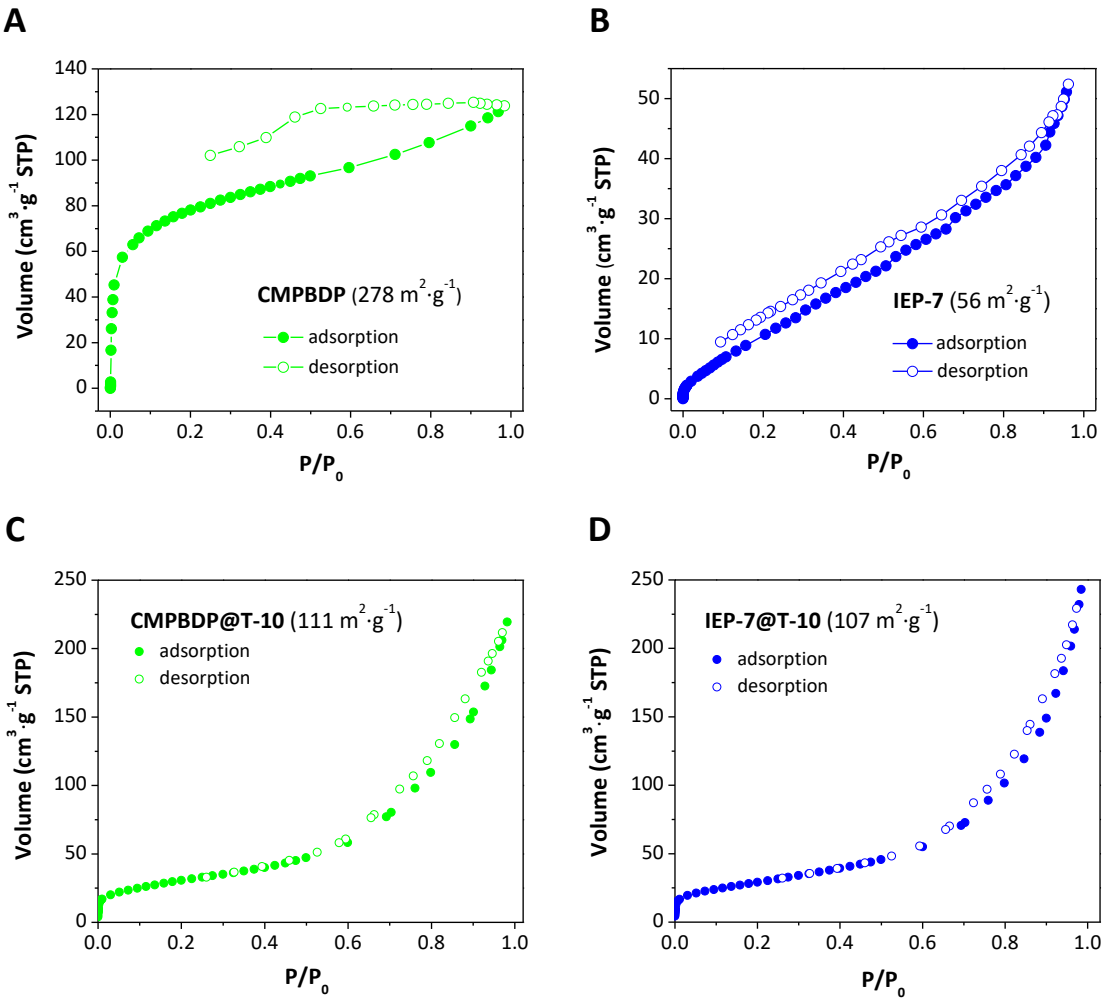

Figure S3. N_2 adsorption/desorption isotherms and BET surface areas of CPPs (**A**-**B**) and CPP@TiO_2 hybrids (**C**-**D**).

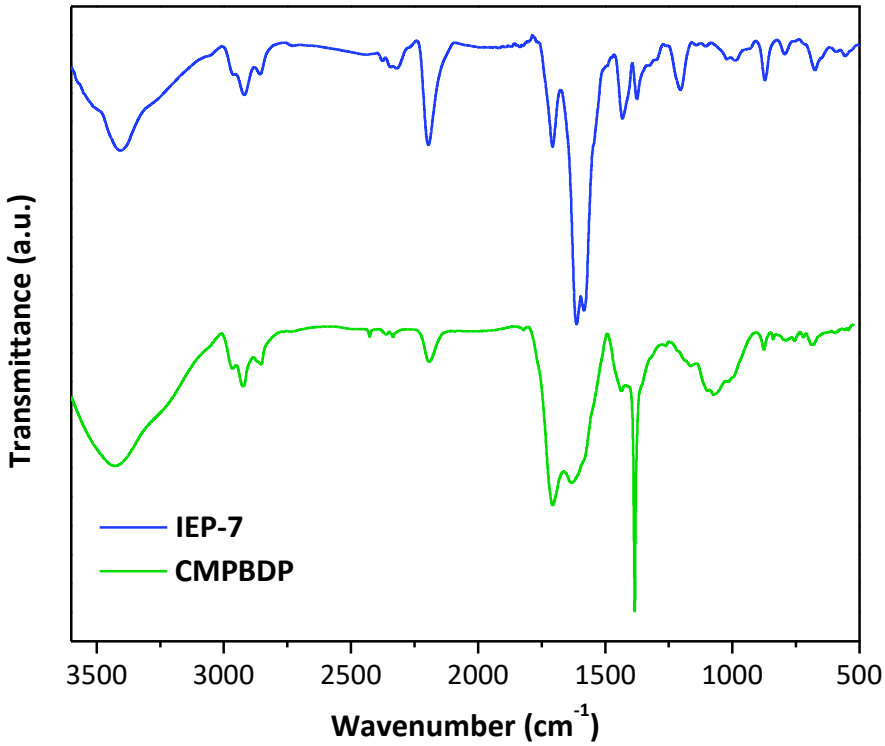

Figure S4. ATR-FTIR spectra of the polymeric networks **IEP-7** and **CMPBDP**.

The FTIR spectra of the BOPHY-based CPP (*i.e.***IEP-7**) shows a C≡C stretching band at *ca.* 2195 cm^{-1} indicative of the condensation between the reactant units, as well as a band at *ca*. 1586 cm^{-1} associated with the BOPHY moiety. On the other hand, the FTIR spectra of **CMPBDP** shows the characteristic bands of the BODIPY dye. Namely, C=N stretching (*ca*. 1629 cm^{-1}), C=C stretching (*ca*. 1200 cm^{-1}), ring skeleton vibrations (*ca*. 1384 cm^{-1}), C≡C stretching (*ca*. 2194 cm^{-1}), and aromatic C−H stretching frequencies up to 3000 cm^{-1}.

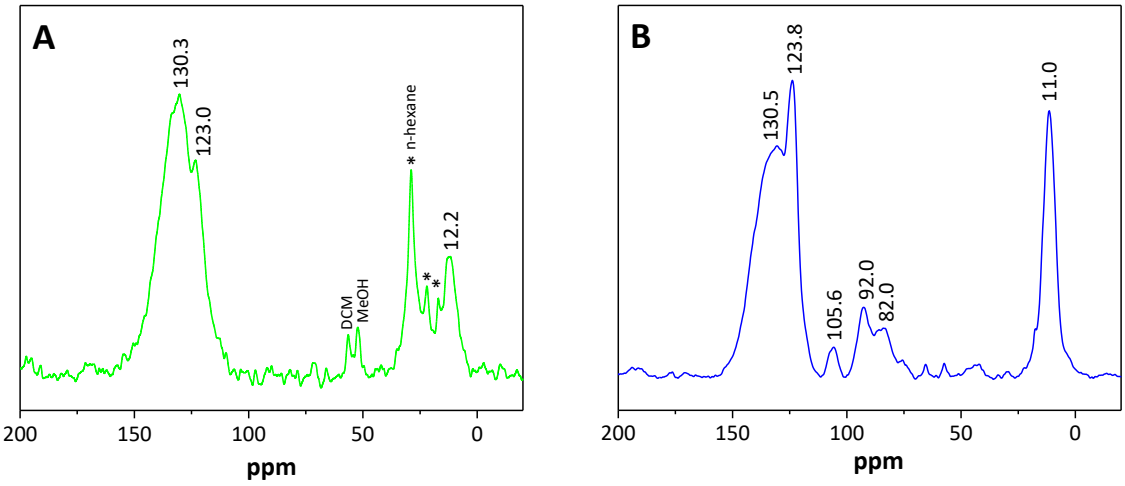

Figure S5. Solid ^{13}C-NMR spectra of **CMPBDP** (**A**) and **IEP-7** (**B**). Additional bands are assigned to solvents from the sample (*i.e.* Dichloromethane (DCM), methanol (MeOH), and n-hexane).

The solid-state ^{13}C NMR spectra of **CMPBDP** (Figure S5A) shows broad peaks between 100−150 ppm due to aromatic carbons atoms, and signals at 5−15 ppm associated with carbon atoms of the methyl groups from the BODIPY moiety. For **IEP-7** (Figure S5B), the signals of aromatic carbons are localized at the interval 105–155 ppm. Besides, two peaks appear at 82 and 92 ppm as a result of the triple bond group, and a narrow peak at 11 ppm related to the aliphatic C from BOPHY moiety.

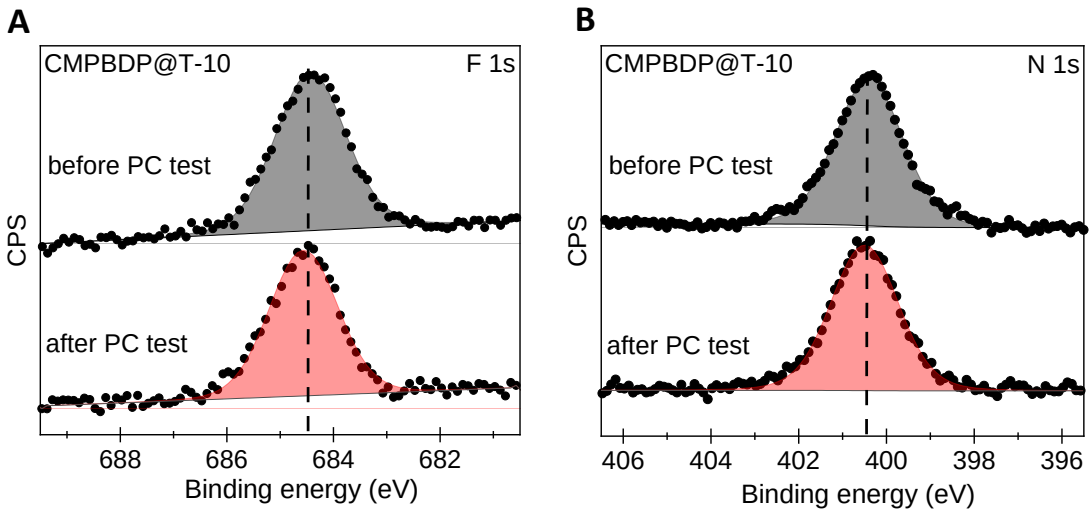

Figure S6. XPS of hybrid samples in the F 1s and N 1s regions before and after a photocatalytic H_2 evolution experiment.

The F 1s region can be fitted with a single Voigt function, with a maximum at 684.5 eV (Figure S6A). This value is significantly lower than the F 1s position found in the spectra of $EtNH_2BF_3$ and Ph_3PBF_3 (686 eV)[2], which is consistent with a higher electron density in the B center of the BF_2 unit in the BODIPY. The N 1s peak (Figure S6B) can also be fitted with a single Voigt function and its position, around 400.5 eV, is within the binding range of N 1s for organic materials.[2] However, the N 1s peak position is slightly higher than those reported for pryridinic (around 398.6 ev) and pyrrolic (around 400.0 eV) compounds.[3] The higher binding energy may be result from a strong interaction with the BF2 center, whose coordination results in a positive charge shared between the two N atoms in the dipyrromethene. Both N 1s and F 1s spectral features remained unaltered after running a photocatalytic test for 5h (Figure S6). An ESCA analysis (*Electron Spectroscopy for Chemical Analysis*) of the F/Ti ratio of the hybrid´s surface, before and after the photocatalytic test, showed that the composition remained constant within the experimental error (*ca.* F:Ti = 2:100).

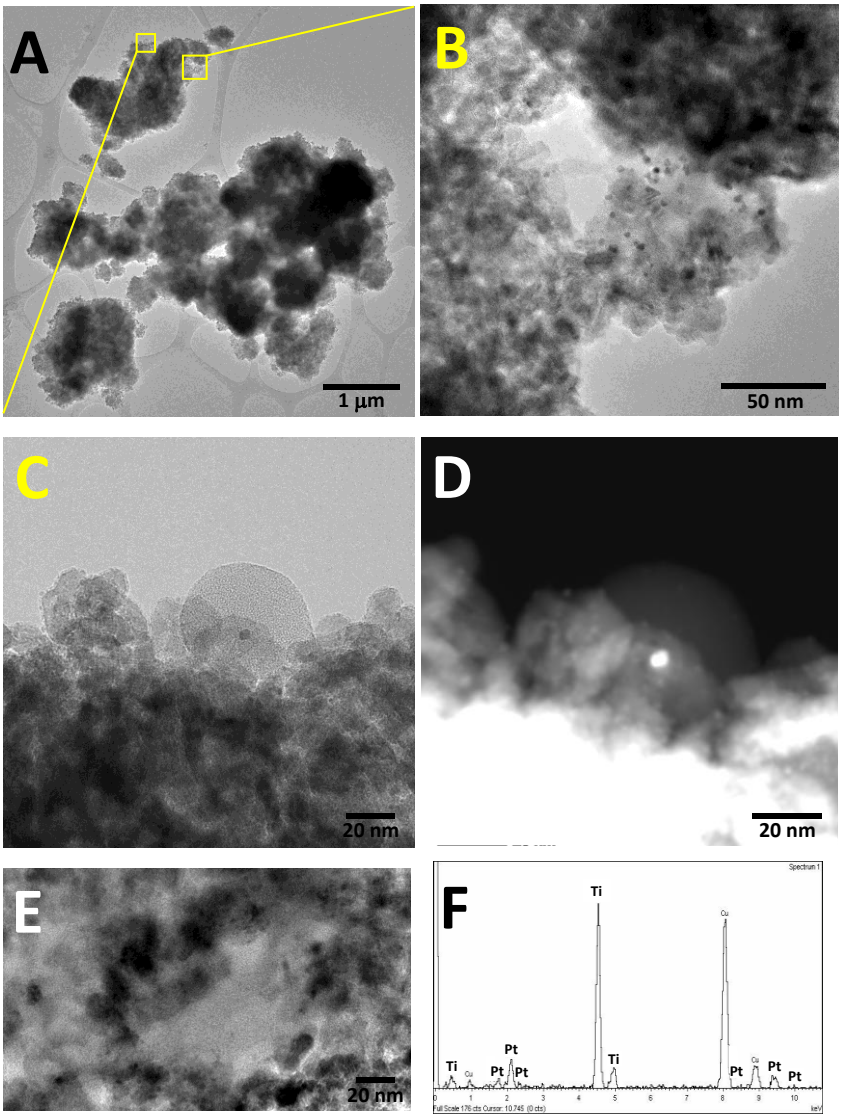

Figure S7. STEM images of Pt/CMPBDP@T-10 hybrid. **B** and **C** depicts a magnification of the squared regions in image **A**; **D** shows the HAADF-STEM image from C; **F** shows the EDS spectrum from region E.

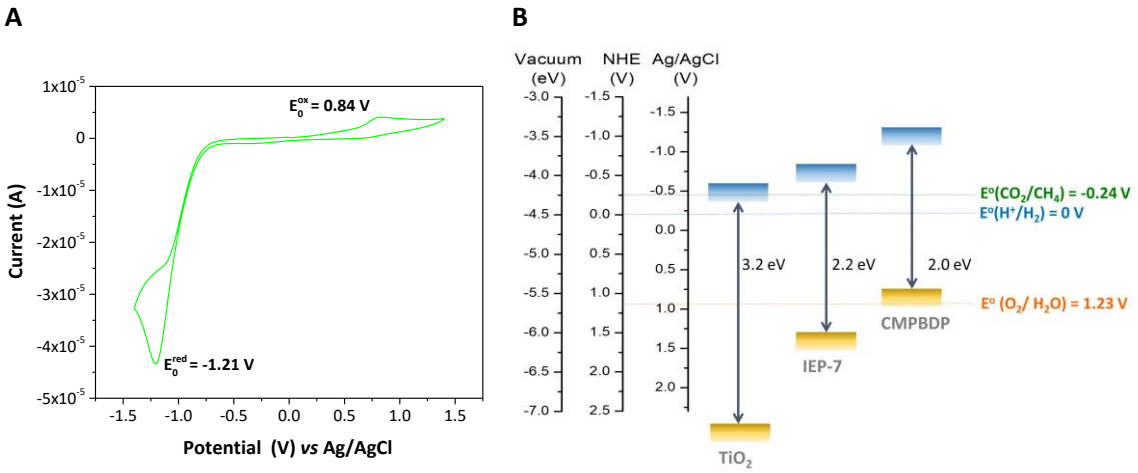

Figure S8. Cyclic voltammetry (CV) of **CMPBDP** measured in acetonitrile containing 0.1M $[(^{n}Bu)_4)N]PF_6$ as electrolyte at a scan rate of 20 mV s^{-1} (**A**); Experimental band energy diagram obtained for CPPs and TiO_2 (note that CV for **IEP-7** and TiO_2 can be found in previous publications[1]), including the water-splitting and CO_2/CH_4 redox couples at pH = 0 (**B**).

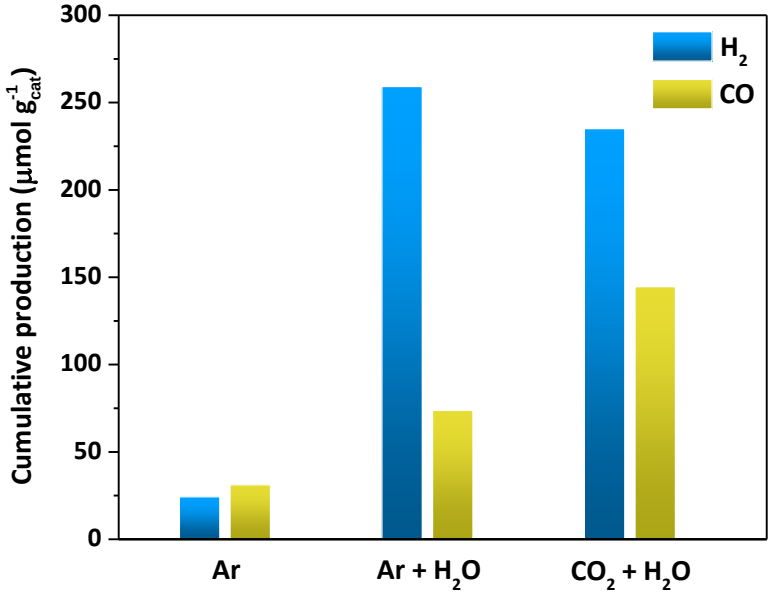

Figure S9. H_2 and CO evolution over the **CMPBDP@T10** hybrid under different reaction atmospheres (i.e. Ar; Ar + H_2O; CO_2+ H_2O) after 15 h of UV illumination.

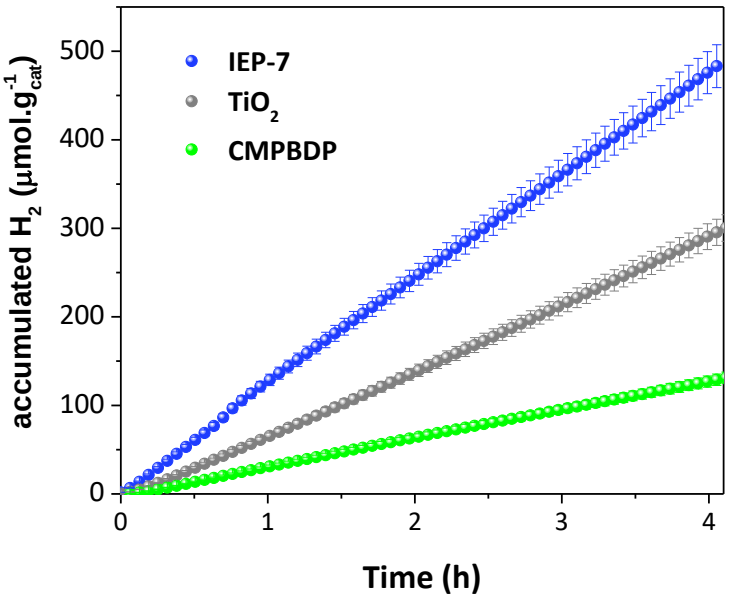

Figure S10. Cumulative hydrogen production *versus* reaction time of CPPs and TiO_2 under UV illumination.

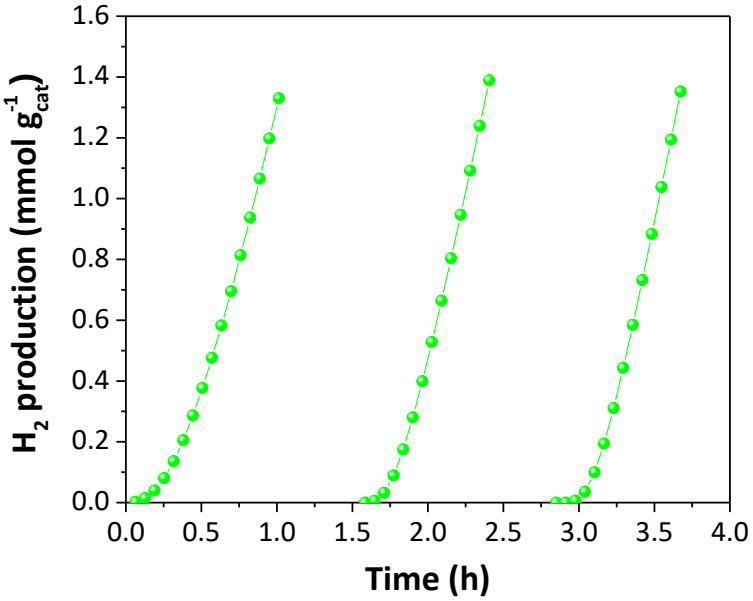

Figure S11. Recyclability of **CMPBDP@T-10** for H_2 production during UV-dark cycles.

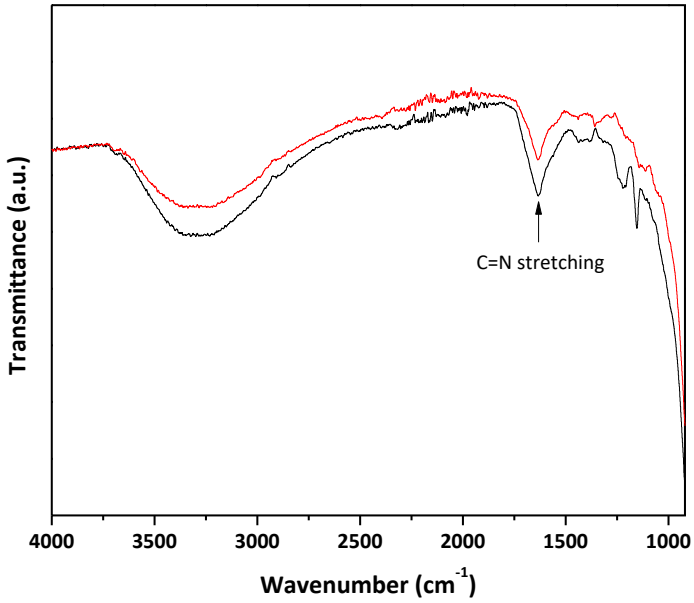

Figure S12. ATR-FTIR spectra of **CMPBDP@T-10** before and after 3 UV-dark cycles of photocatalytic H_2 evolution tests.

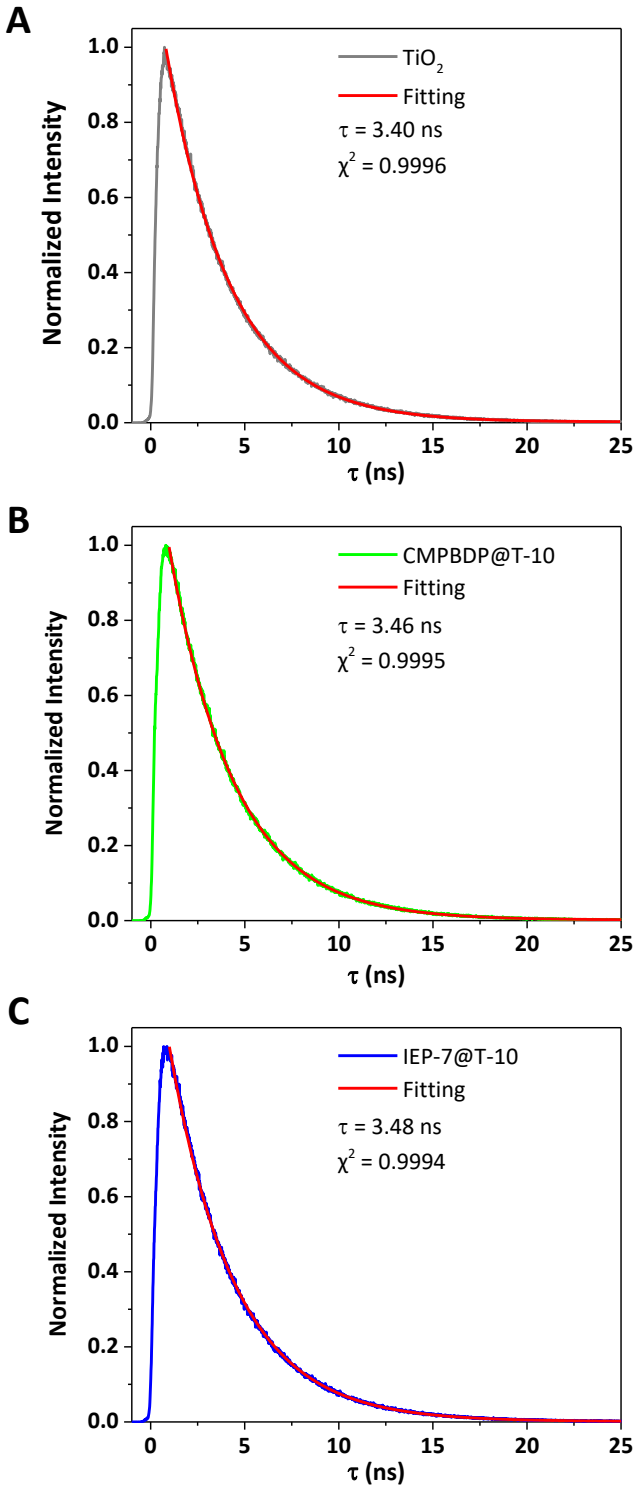

Figure S13. Normalized fluorescence decay traces (λ_{exc} = 372 nm, cut-off filter centered at 450 nm) for TiO_2 (**A**) and the hybrids **CMPBDP@T-10** (**B**) and **IEP-7@T-10** (**C**) measured in solid state. The fitting curves (red) have been included in all cases.

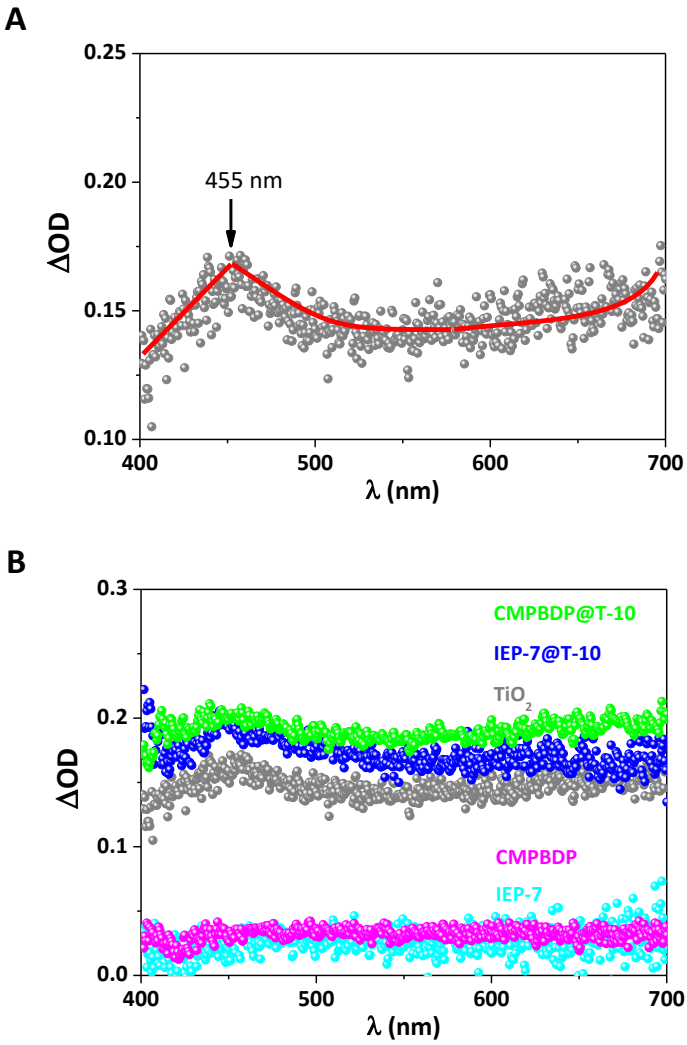

Figure S14. A) Transient absorption spectra (TAS, λ_{exc} = 355 nm) for TiO_2 measured in suspension solution under inert atmosphere. **B**) TAS for TiO_2 (grey), the hybrids **CMPBDP@T-10** (green) and **IEP-7@T-10** (blue), and the comparison with their bare materials **CMPBDP** and **IEP-7** (magenta and cyan, respectively) under the same conditions.

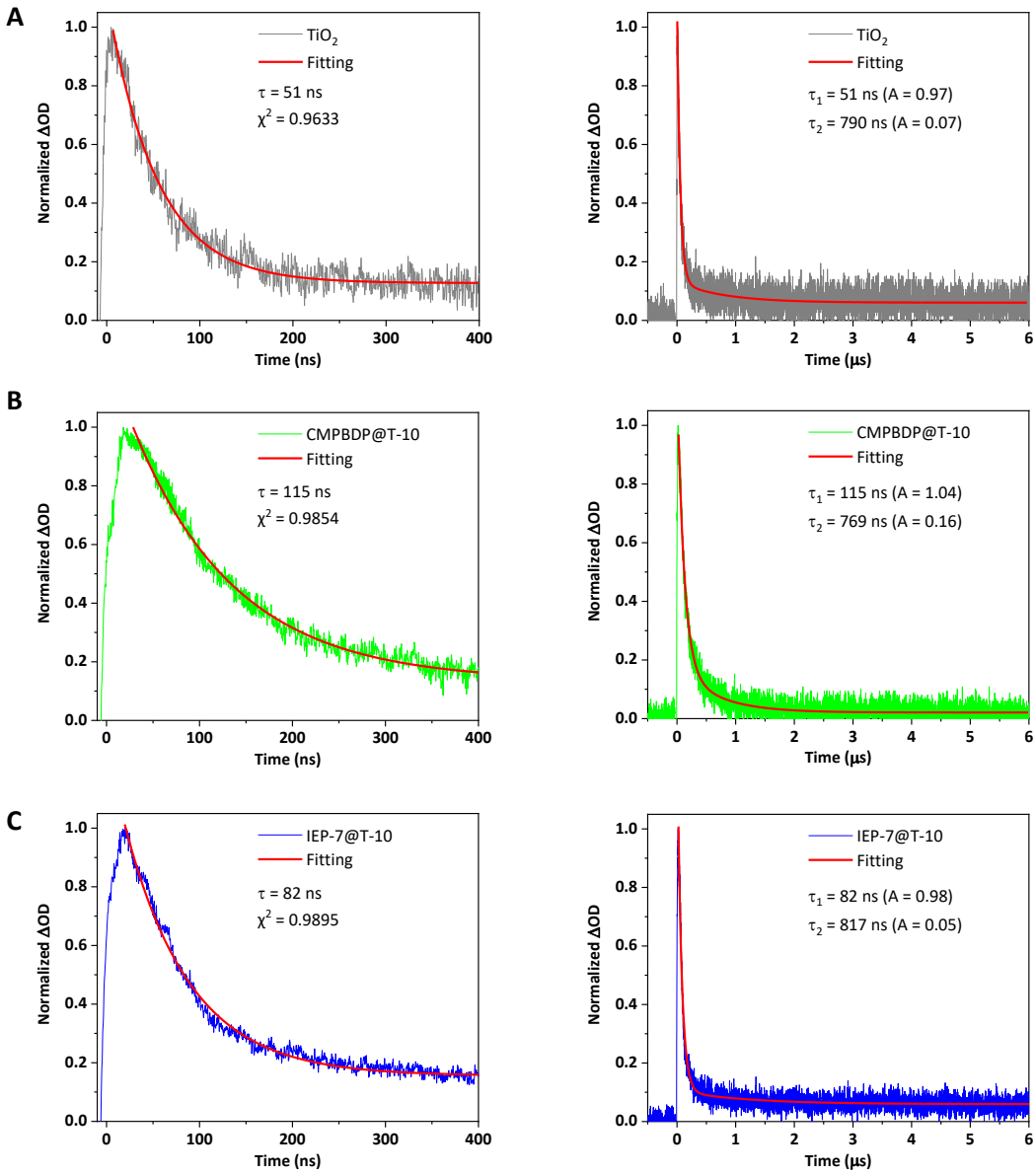

Figure S15. Fits of the normalized transient decay traces (λ_{exc} = 355 nm, λ_{obs} = 460 nm) monitored up to 400 ns after laser pulse (left side) or until 6 μs (right side) for **A**) TiO_2, **B**) **CMPBDP@T-10** and **C**) **IEP-7@T-10**.

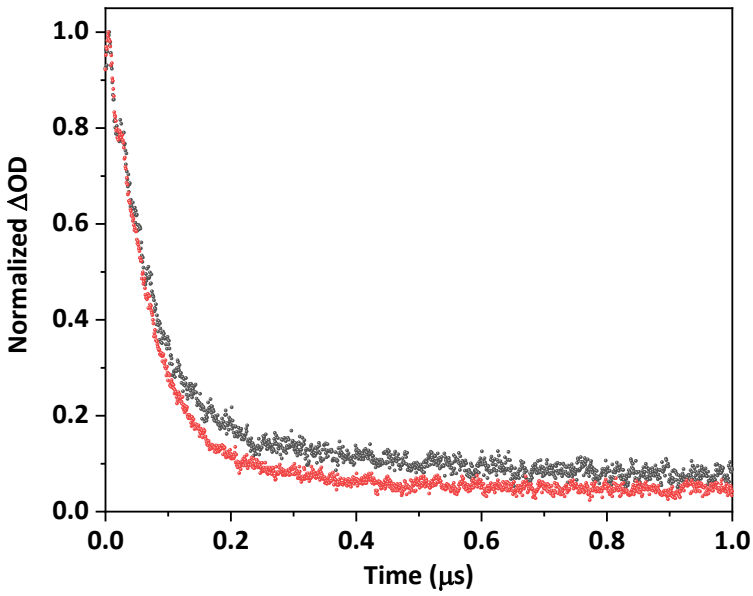

Figure S16. Decay traces (λ_{exc} = 355 nm, λ_{obs} = 460 nm) for deaerated TiO_2 in the absence (red) or presence (black) of 10% vol. MeOH aqueous suspensions.

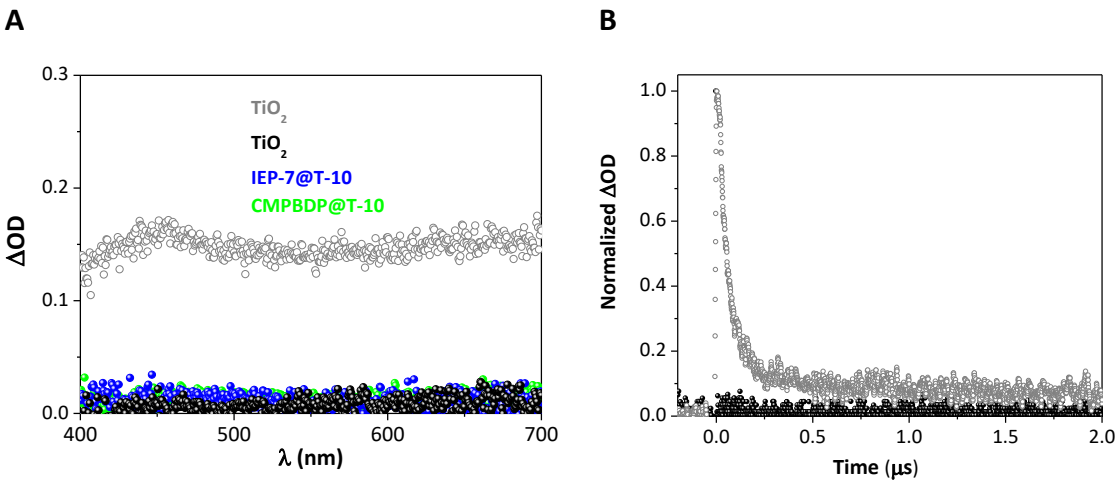

Figure S17. A) TAS (λ_{exc} = 355 nm) for TiO_2 in the absence (grey, open circles) or in the presence (black circles) of H_2PtCl_6 as electron scavenger. TAS for **CMPBDP@T-10** (green) and **IEP-7@T-10** (blue) in the presence of H_2PtCl_6 have been included for comparative purposes; **B**) Decay traces (λ_{exc} = 355 nm, λ_{obs} = 460 nm) for deaerated TiO_2 in absence (grey) or presence (black) of H_2PtCl_6.

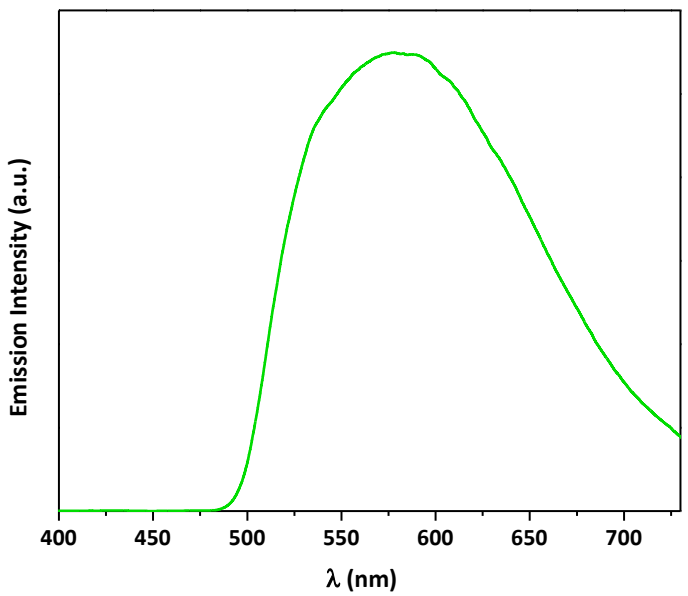

Figure S18. Solid-state photoluminescence spectra of **CMPBDP** (λ_{exc} = 445 nm, cut-off filter at 450 nm).

Table S1. Surface composition of **CMPBDP@T-10** based on X-ray photoelectron spectra before and after a photocatalytic H_2 production test.

	N : F : TiO_2 surface atomic ratio[a]	**N : F : TiO_2 nominal atomic ratio**[b]
CMPBDP@T-10 as prepared	1.2 : 2 : 100	4.3 : 4.3 : 100
CMPBDP@T-10 after reaction	1.4 : 2 : 100	

[a]Based on the N 1s, F 1s and Ti 2p peaks areas and their respective sensitivity factors.

[b]Derived from the nominal composition of the hybrid, 10%w/w of the polymer.

The concentration of N and F on the surface is lower than expected for the nominal composition of the hybrid. This suggests the TiO_2 particles are preferentially located at the surface of the hybrid.

Table S2. Cumulative CO_2 photoreduction productions after 15 h of UV illumination for hybrid heterojunctions (i.e. **CMPBDP@T-10**, **IEP-7@T-10**), bare polymer (i.e. **CMPBDP**) and TiO_2. Photonic efficiencies towards CH_4 are also included for comparison.

	Cumulative production (μmol g_{cat}^{-1})						**Photonic efficiency, ʒ (%) to CH_4**
	H_2	**CO**	**CH_4**	**$C_2H_4O_2$**	**C_2H_4**	**C_2H_6**	
CMPBDP@T-10	235.1	144.6	60.3	1.6	5.4	8.3	0.13
CMPBDP	20.4	11.3	0.0	38.7	0.0	0.0	0.00
IEP-7@T-10	241.7	129.3	43.6	2.2	3.2	6.5	0.09
TiO_2	63.8	124.9	15.4	2.1	0.8	0.8	0.04

Table S3. Some relevant examples of organic-inorganic hybrid materials based on TiO_2 and polymers for CO_2 photoreduction.

IS	Polymer	Cocatalyst	Reactor	Preparation details	Morphology	Light source	Charge transfer mechanism[a]	Rate (units)	AQY[b] or ξ[c] (%), (λ (nm))	Ref Year
TiO_2 (PC500)	CMPBDP[d]	N/A	Gas-solid	Physical mixture and grinding	TiO_2 nanocrystals surrounding polymer network	4 UV lamps (6W) (λ_{max} = 369nm)	Type II Heterojunction	CO: 15.1 μmol g^{-1} h^{-1} CH_4: 6.9 μmol g^{-1} h^{-1} H_2: 26.3 μmol g^{-1} h^{-1} 4.1 (CH_4) and 4.4 (H_2) times higher than TiO_2	0.13[f](369)	**This work 2021**
TiO_2 (PC500)	IEP-7[e]	N/A	Gas-solid	Physical mixture and grinding	TiO_2 nanocrystals surrounding polymer network	4 UV lamps (6W) (λ_{max} = 369nm)	Type II Heterojunction	CO: 12.2 μmol g^{-1} h^{-1} CH_4: 5.0 μmol g^{-1} h^{-1} H_2: 23.7 μmol g^{-1} h^{-1} 3 (CH_4) and 4 (H_2) times higher than TiO_2	0.09[f] (369)	**This work 2021**
TiO_2	PVDF[g]	N/A	Gas-solid	TiO_2 nanocrystals synthesized over electrospinned polymer	Composite	4 UVA lamps (8W) (λ_{max} =365nm)	N/A	CO: 15.1 μmol g^{-1} h^{-1} CH_4: 3.1 μmol g^{-1} h^{-1}	N/A	[4] 2019
TiO_2-functionalized graphene	HCP[h]	N/A	Gas-solid	Hypercrosslinked polymer synthesized over TiO_2-graphene composite	Composite	Xe lamp (≥420nm)	Sensitization	CO: 21.6 μmol g^{-1} h^{-1} CH_4: 27.6 μmol g^{-1} h^{-1}	N/A	[5] 2019
TiO_2	PDA[i]	N/A	Gas-solid	PDA (1 nm of coating) synthesized over TiO_2 surface	Polymer coating	Xe lamp (>400nm)	Sensitization	CO: 3.0μmol g^{-1} h^{-1}	N/A	[6] 2018

Table S3. Cont. Some relevant examples of organic-inorganic hybrid materials based on TiO_2 and polymers for CO_2 photoreduction.

IS	Polymer	Cocatalyst	Reactor	Preparation details	Morphology	Light source	Charge transfermechanism[a]	Rate (units)	AQY[b] or ξ[c] (%), (λ (nm))	Ref (Year)
TiO_2	B-doped g-C_3N_4[j]	N/A	Gas-liquid	TiO_2 synthesized by sol-gel over polymer	Composite	Xe lamp (≥420nm)	Sensitization	CH_4: 131.3 μmol g^{-1} h^{-1}	1.68, (420)	[7] 2016
TiO_2 (P25)	PANI[k]	0.2 wt.% Pt	Gas-solid	In situoxidative polymerization of PANI	Polymer coating	Xe lamp (320–780 nm)	N/A	CH_4: 50.0μmol g^{-1} h^{-1} H_2: 320.0 μmol g^{-1} h^{-1} 3.3 (CH_4) and 2.8 (H_2) times higher than Pt/TiO_2	N/A	[8] 2015
N-TiO_2[l]	g-C_3N_4[j]	N/A	Gas-solid	Thermal treatment with urea and $Ti(OH)_4$ (7:3) wt/wt	Composite	Xe lamp (UV-Vis)	Type II Heterojunction	CO: 11.9 μmol g^{-1} h^{-1} 4 times higher than P25	N/A	[9] 2014

[a]Here we include the charge transfer mechanism as named in the original scientific paper. Note that Type II and p–n junction refer to the same mechanism; [b]AQY, Apparent Quantum Yield, AQY (%) = (Number of reacted electrons)/ (Number of incident photons) × 100%; [c]ξ, Photonic Efficiency calculated as the ratio between the rate of reaction and the incident photon flux; [d]Conjugated microporous polymer based on a BODIPY dye; [e]IMDEA Energy Polymer number 7 consisting on a conjugated porous polymer based on a BOPHY dye; [f]Photonic efficiency towards CH_4; [g]Polyvinylidene fluoride; [h]Hypercrosslinked polymer; [i]Polydopamine; [j]Graphitic carbon nitride; [k]Polyaniline; [l]N-doped TiO_2 nanofibers.

Table S4. Some relevant examples of organic-inorganic hybrid materials based on $TiO_2$for photocatalytic hydrogen production from water.

IS	CP	Co-catalyst	Sacrificial Agent	Light source	Charge transfer mechanism[a]	Formation rate (mmol g^{-1} h^{-1})	AQY[b] or ξ[c] (%), (λ (nm))	Ref
TiO_2	**CMPBDP**	**1 wt.% Pt**	**10 vol.% MeOH aq.**	**Hg lamp**	**Type II**	**56.4**	**20.43[c]**	**This work**
TiO_2	IEP-7	1 wt.%Pt	10 vol.% MeOH aq.	Hg lamp	Type II	39.3	14.54	[10]
TiO_2	TxPPT	1 wt.% Pt	10 vol.% MeOH aq.	Hg lamp	Z-scheme	21.9	N/A	[11]
TiO_2	Polycatechol	N/A	5 vol.% TEOA aq.	Solar light	LMCT[d]	10.9	N/A	[12]
TiO_2	B-BT-1,4-E	0.03 wt.% residual Pd	TEOA aq.	Xe-lamp (λ ≥ 420 nm)	Sensitization	7.3	1.91 (420)	[13]
TiO_2	B-BT-1,4-E	1 wt.% Au	10 vol.% TEOA	Xe-lamp (λ ≥ 420 nm)	Sensitization	26.6	7.8 (420)	[14]
Black TiO_2	B-BT-1,4-E	residual Pd	10 vol.% TEOA	Xe-lamp (λ ≥ 420 nm)	Type II heterojunction	15.6	3.36 (420)	[15]
TiO_2	BFB or BFBA	0.4 wt.% residual Pd	TEOA aq.	Xe-lamp (λ ≥ 420 nm)	Sensitization	3.7 7.3	1.6 (420) 2.46 (420)	[16]
TiO_2	CMPBBT	0.5 wt.% Pt	TEOA	Xe-lamp (λ ≥ 420 nm)	Sensitization	5.9	N/A	[17]
TiO_2[e]	COP64	3 wt.% Pt	10 vol.% MeOH aq.	Xe-lamp (without UV cut-off filter)	p-n junction	15.0	N/A	[18]
TiO_2	TpTph	3.9 wt. % Pt	Ascorbic acid	Xe-lamp (λ ≥ 420 nm)	Sensitization	5.6	N/A	[19]
N-TiO_2[f]	g-C_3N_4	Pt (amount no provided)	20 vol.% MeOH aq.	Simulated solar light	p-n junction	8.9	N/A	[20]

Table S4. Cont. Some relevant examples of organic-inorganic hybrid materials based on TiO_2 used in photocatalytic hydrogen production from water.

IS	CP	Co-catalyst	Sacrificial Agent	Light source	Charge transfer mechanism[a]	Formation rate (mmol g^{-1} h^{-1})	AQY[b] or ξ[c] (%), (λ (nm))	Ref
TiO_2	B-doped g-C_3N_4	N/A	20 vol.% MeOH aq.	Xe-lamp (λ ≥ 420 nm)	Sensitization	0.2	3.08 (420)	[7]
Black-TiO_2	g-C_3N_4	N/A	20 vol.% MeOH aq.	Simulated solar light	Type II	0.6	N/A	[21]
TiO_2	TbBD-COF	3 wt.% Pt	10 vol.%TEOA aq	Xe-lamp	Type II	0.004	N/A	[22]

[a]Here we include the charge transfer mechanism as named in the original scientific paper. Note that Type II and p–n junction refer to the same mechanism; [b]AQY, Apparent Quantum Yield, AQY (%) = (2× Number of evolved H_2 molecules)/ (Number of incident photons) × 100%; [c]ξ, Photonic Efficiency calculated as the ratio between the rate of reaction and the incident photon flux; [d]LMCT:Ligand to Metal Charge Transfer; [e]TiO_2 Nanosheet; [f]N-doped TiO_2 nanofibers.

REFERENCES

[[1] C. G. López-Calixto, S. Cabrera, R. Pérez-Ruiz, M. Barawi, J. Alemán, V. A. de la Peña O'Shea, M. Liras, *Appl. Catal. B Environ.* **2019**, *258*, 117933.

[2] C. D. Wagner, W. M. Riggs, L. E. Davis, J. F. Moulder, *Handbook of X-Ray Photoelectron Spectroscopy* (Ed.: Muilenberg, G. E.), Perkin-Elm., **1979**.

[3] D. Y. Osadchii, A. I. Olivos-Suarez, A. V. Bavykina, J. Gascon, *Langmuir* **2017**, *33*, 14278.

[4] P. Dong, Z. Huang, X. Nie, X. Cheng, Z. Jin, X. Zhang, *Mater. Res. Bull.* **2019**, *111*, 102.

[5] S. Wang, M. Xu, T. Peng, C. Zhang, T. Li, I. Hussain, J. Wang, B. Tan, *Nat. Commun.* **2019**, *10*, 676.

[6] T. Wang, M. Xia, X. Kong, *Catalyst* **2018**, 215.

[7] F. Raziq, Y. Qu, X. Zhang, M. Humayun, J. Wu, A. Zada, H. Yu, X. Sun, L. Jing, *J. Phys. Chem. C* **2016**, *120*, 98.

[8] G. Liu, S. Xie, Q. Zhang, Z. Tian, Y. Wang, *Chem. Commun.* **2015**, *51*, 13654.

[9] S. Zhou, Y. Liu, J. Li, Y. Wang, G. Jiang, Z. Zhao, D. Wang, A. Duan, J. Liu, Y. Wei, *Appl. Catal. B Environ.* **2014**, *158–159*, 20.

[10] C. G. López-Calixto, M. Barawi, M. Gomez-Mendoza, F. E. Oropeza, F. Fresno, M. Liras, V. A. de la Peña O'Shea, *ACS Catal.* **2020**, *10*, 9804.

[11] A. Valverde-González, C. G. López Calixto, M. Barawi, M. Gomez-Mendoza, V. A. De La Peña O'Shea, M. Liras, B. Gómez-Lor, M. Iglesias, *ACS Appl. Energy Mater.* **2020**, *3*, 4411.

[12] P. Karthik, R. Vinoth, P. Selvam, E. Balaraman, M. Navaneethan, Y. Hayakawa, B. Neppolian, *J. Mater. Chem. A* **2017**, *5*, 384.

[13] Y. Xiang, X. Wang, X. Zhang, H. Hou, K. Dai, Q. Huang, H. Chen, *J Mater Chem A* **2018**, *6*, 153.

[14] J. Xiao, Y. Luo, Z. Yang, Y. Xiang, X. Zhang, H. Chen, *Catal. Sci. Technol.* **2018**, *8*, 2477.

[15] X. Zhang, J. Xiao, C. Peng, Y. Xiang, H. Chen, *Appl. Surf. Sci.* **2019**, *465*, 288.

[16] B. Chen, X. Wang, W. Dong, X. Zhang, L. Rao, H. Chen, D. Huang, Y. Xiang, *Chem. - A Eur. J.* **2019**, *25*, 3362.

[17] H. Hou, X. Zhang, D. Huang, X. Ding, S. Wang, X. Yang, S. Li, Y. Xiang, H. Chen, *Appl. Catal. B, Environ.* **2017**, *203*, 563.

[18] Q. Yang, P. Peng, Z. Xiang, *Chem. Eng. Sci.* **2017**, *162*, 33.

[19] G. Mukherjee, J. Thote, H. B. Aiyappa, S. Kandambeth, S. Banerjee, K. Vanka, R. Banerjee, *Chem. Commun.* **2017**, *53*, 4461.

[20] C. Han, Y. Wang, Y. Lei, B. Wang, N. Wu, Q. Shi, Q. Li, *Nano Res.* **2015**, *8*, 1199.

[21] L. Shen, Z. Xing, J. Zou, Z. Li, X. Wu, Y. Zhang, Q. Zhu, S. Yang, W. Zhou, *Sci. Rep.* **2017**, *7*, 1.

[22] L. Liu, J. Zhang, X. Tan, B. Zhang, J. Shi, X. Cheng, D. Tan, B. Han, L. Zheng, F. Zhang, *Nano Res.* **2020**, *13*, 983.